



Published in final edited form as:

Dev Cell. 2008 July ; 15(1): 146–162. doi:10.1016/j.devcel.2008.05.003.

Cytoskeletal Dynamics Underlying Neurite Outgrowth

Andrew W Schaefer^{1,3}, Vincent Th.G. Schoonderwoert^{1,3}, Lin Ji², Nelson Mederios, Gaudenz Danuser², and Paul Forscher^{1,*}

¹Dept. of Molecular, Cellular and Developmental Biology, Yale University, New Haven CT 06511

²Dept of Cell Biology, Scripps Research Institute (TSRI), La Jolla, CA 92037

Abstract

Although much evidence suggests that axon growth and guidance depend on well-coordinated cytoskeletal dynamics, direct characterization of the corresponding molecular events has remained a challenge. Here, we address this outstanding problem by examining neurite outgrowth stimulated by local application of cell adhesion substrates. During acute outgrowth, the advance of organelles and underlying microtubules into the central domain was correlated with regions of attenuated retrograde actin network flow in the periphery. Interestingly, as adhesion sites matured, contractile actin arc structures, known to be regulated by the Rho/Rho Kinase/myosin II signaling cascade, became more robust and coordinated microtubule movements in the growth cone neck. When Rho Kinase was inhibited, although growth responses occurred with less of a delay, microtubules failed to consolidate into a single axis of growth. These results reveal a new role for Rho Kinase and myosin II contractility in regulation of microtubule behavior during neuronal growth.

Keywords

growth cone; actin dynamics; microtubule dynamics; motility; adhesion; axon guidance; neuron

Introduction

Neurite outgrowth is thought to involve a stereotypical sequence of events including, 1) protrusion of the growth cone peripheral (P) domain, 2) “engorgement” of the P-domain with organelles from the central (C) domain, and, 3) consolidation of the recently advanced C-domain into the distal segment of the neurite shaft (Goldberg and Burmeister, 1986). Many studies have implicated actin filament and microtubule (MT) dynamics as well as interactions between these two major cytoskeletal polymers in neurite outgrowth and axon guidance (Bentley and O’Connor, 1994; Bentley and Toroian-Raymond, 1986; Bridgman et al., 2001; Buck and Zheng, 2002; Dent and Gertler, 2003; Letourneau et al., 1987; Sabry et al., 1991; Schaefer et al., 2002; Zhou et al., 2002). Evidence suggests assembly of actin filaments in the growth cone is essential for axon guidance (Bentley and Toroian-Raymond, 1986; Challacombe et al., 1996), but is not a formal requirement for axon growth (Marsh and Letourneau, 1984). MTs, on the other hand, play key roles in axon structure and in organelle transport. In addition, MTs have an intriguing but less well understood role in growth cone

*Corresponding author: Paul Forscher, Dept. of Molecular, Cellular and Developmental Biology, Yale University, New Haven CT 06520, Tel: 203-432-6344, Fax: 203-432-8999, Email: paul.forscher@yale.edu.

³Equal contributions to this work

Publisher's Disclaimer: This is a PDF file of an unedited manuscript that has been accepted for publication. As a service to our customers we are providing this early version of the manuscript. The manuscript will undergo copyediting, typesetting, and review of the resulting proof before it is published in its final citable form. Please note that during the production process errors may be discovered which could affect the content, and all legal disclaimers that apply to the journal pertain.

motility related to their “dynamic instability” -the ability MTs have of stochastically switching between growing, paused, and shrinking states (Mitchison and Kirschner, 1984).

Dynamic MTs were initially found to be a prerequisite for persistent growth cone advance and recognition of substrate bound guidance cues (Challacombe et al., 1997; Tanaka et al., 1995; Tanaka and Kirschner, 1995). Recent related evidence suggests that interactions between MTs and actin filaments and signaling cross-talk between Rho family GTPases may be required for a wide range of processes including directed epithelial cell motility, wound healing and axon guidance (Lee et al., 2004; Rodriguez et al., 2003). Despite recent progress characterizing axon guidance signaling pathways (Guan and Rao, 2003) and the roles Rho GTPases play in this process (Gallo and Letourneau, 2004; Huber et al., 2003), the basic cytoskeletal mechanisms underlying axon growth remain poorly understood.

In *Aplysia* growth cones, acute periods of neurite advance, similar to those elicited by native substrates (Bridgman et al., 2001; Lin and Forscher, 1993; Lin et al., 1994; Sabry et al., 1991), can be triggered by application of silica beads coated with the homophilic Ig superfamily molecule apCAM if beads are physically restrained to permit development of traction force (Suter et al., 1998). Growth cone responses to restrained apCAM beads have two distinct phases. The initial “latency” phase begins after bead restraint and is characterized by few overt structural changes other than localized actin assembly near the bead binding site that leads to formation of actin structures which appears to act as a scaffold for docking signaling proteins such as src family kinase(s) involved in regulating adhesion (Suter and Forscher, 2001). The second or “growth” phase appears to be characterized by slowing of retrograde actin flow in the corridor where directed C-domain advance occurs (Lin and Forscher, 1995; Suter et al., 1998).¹ Retrograde flow attenuation is followed by a gradual increase in tension between the restrained bead substrate and the growth cone consistent with published reports of force generation during neurite outgrowth (Bray, 1979; Lamoureux et al., 1989).

The above observations suggested a “molecular clutch” model for growth cone advance where traction force results from stiffening of the linkage between restrained apCAM substrates and underlying actin networks undergoing retrograde flow (Suter and Forscher, 2000). However, the cytoskeletal mechanism implied by this model has never been directly tested since previous studies relied on indirect assessment of actin network movements using surface bound flow coupled bead markers. Those studies provided limited insight into how changes in actin structure actually promote MT and C-domain advance. Moreover, they could not readily distinguish between changes in actin network movement and actin network disruption. In both cases surface bound beads could stop moving rearward but the underlying mechanisms would be quite different.

Earlier studies also did not identify the cytoskeletal effectors responsible for adhesion dependent tension. Actin-myosin II structures localized in the transition zone (T-zone) between the C and P domains of vertebrate growth cones are a possible candidate (Bridgman, 2002; Lewis and Bridgman, 1992). In *Aplysia* growth cones, actin-myosin II structures termed “actin arcs” play a role in driving peripheral retrograde flow and actin bundle recycling in the T zone (Medeiros et al., 2006). Interestingly, actin arcs along the sides of the growth cone align with MTs and actively transport them from the periphery into the the C-domain (Schaefer et al., 2002). Evidence suggests actin arcs contribute to the Rho Kinase dependent contractility of the C-domain (Zhang et al., 2003).

¹We previously referred to the acute period of C-domain advance as the “interaction phase” (Suter et al., 1998). We feel substrate evoked “growth phase” more accurately describes this phenomenon and will use this terminology here and in the future.

In the current study we used fluorescent speckle microscopy (FSM) (Waterman-Storer et al., 1998) and automated adaptive fluorescent feature tracking (Danuser and Waterman-Storer, 2006) to assess actin filament and microtubule polymer dynamics during periods of neurite advance evoked by cell adhesion molecule substrates. We report the first direct visualization of the cytoskeletal “system response” underlying neurite advance and investigate new roles for actin turnover and Rho Kinase dependent contractility.

Results

Actin Filament Dynamics Underlying Substrate Evoked Growth

Neurons were injected with Alexa-594 phalloidin at low levels appropriate for generating internal reference marks or “speckle” features to assess actin filament dynamics as previously described (Schaefer et al., 2002). Fluorescent phalloidin was used, as opposed to G-actin, because it generates higher contrast actin filament structures and has no significant effect on filament turnover at the low concentrations used. Total internal reflection fluorescence (TIRF) imaging was employed because it provides high signal/noise imaging of cytoskeletal dynamics and significantly lower phototoxicity relative to conventional epifluorescence (Zhang et al., 2003). This enabled the long recordings necessary to capture substrate evoked growth responses reported here. Since fluorescence excitation in TIRF imaging is limited to a narrow evanescent wave zone, structures $> \sim 200$ nm above the cover-slip surface illuminated field are not visualized. We controlled for the possibility of missing relevant structural changes by periodically bringing the microscope out of TIRF and into epifluorescence imaging mode during targeting responses to verify the presence or absence of structures (AWS, VTS, unpublished observations). Cytoskeletal dynamics were correlated with morphological changes by differential interference contrast (DIC) imaging.

After allowing time for fluorescent cytoskeletal probe incorporation, apCAM bead substrates were applied individually to the dorsal surface of the growth cone P-domain and restrained from movement by retrograde actin flow using a micro-needle as described (Suter et al., 1998; Suter and Forscher, 2001). A growth cone 280 sec into the latency phase of a target interaction is shown in Fig. 1A. During this initial period no significant changes in the distribution of organelles in the C-domain are observed; however, membrane ruffling formation indicative of local actin filament assembly (Suter et al., 1998) and recruitment of signaling proteins (Suter and Forscher, 2001) can be seen around the restrained bead (Fig. 1A white arrowheads). Ruffling can best be visualized in the DIC channel of movies S1, S4, and S5 and appears as raised membrane trailing off from the bead in the direction of retrograde flow.

Radial arrays of actin bundles embedded in the actin meshwork of the P-domain (Lewis and Bridgman, 1992; Schaefer et al., 2002) are evident in the corresponding F-actin image (Fig. 1B, star). These bundles form the cores of filopodia which typically do not extend far beyond the peripheral actin meshwork in our culture conditions. Note the radial bundles are present in the future target interaction axis (Fig. 1A, double arrow). Phalloidin does not appear to label actin assembly dependent membrane ruffling near the bead target in live cell imaging (compare Fig. 1A with 1B, white arrowheads) suggesting actin filaments near the bead adhesion site have a turnover rate that is fast relative to the slow on rate constant for phalloidin binding (De La Cruz and Pollard, 1996; Zhang et al., 2003).

Retrograde actin flow moves actin networks assembled at the leading edge rearward across the P-domain at rates of $3\text{--}6 \mu\text{m min}^{-1}$ and into the T-zone where flow slows (Forscher and Smith, 1988; Schaefer et al., 2002) and the ends of filopodial cores reside (Fig. 1B, green arrowhead). With the exception of intrapodia activity near the target bead, throughout the latency period

no morphological changes or alterations in the overall organization of F-actin structure were observed and retrograde actin flow in the P-domain remained relatively constant.

In previous studies we used kymographs for analysis of actin movements (Schaefer et al., 2002). However, kymography is useful only in regions of uniform flow directionality, and is poorly suited for global characterization of actin dynamics where actin flow patterns are more complex. To address this problem, an automated cross-correlation algorithm for detecting and measuring actin flow fields was developed (Hu et al., 2007; Ji and Danuser, 2005). This approach permits complete characterization of actin flow rates in all directions in each domain and across domain transitions. Regional flow trajectories and magnitudes are averaged over 30-36s and quantitatively represented by the vectors in each flow field. A typical F-actin flow field recorded during the latency period is shown in Fig. 1C and exhibits the same general flow characteristics as control growth cones before bead placement (Supp Figs. 1 and 2). Flow rates in the P-domain were $\sim 6.4 \mu\text{m min}^{-1}$ and decreased as filaments approached and moved through the T-zone into the C-domain. Note that during the latency period retrograde actin flow is uniformly fast across the radial extent of the P-domain including the future target interaction axis. During this period, when F-actin flow trajectories tended to be centripetal and linear, we found close agreement with rates assessed previously by manual tracking of speckle features (Schaefer et al., 2002).

During the growth phase (also referred to as C-domain “engorgement” of the periphery (Goldberg and Burmeister, 1986) directed advance of the C-domain toward the apCAM bead binding site was observed. During this period, the distal C-domain focuses into a bullet-like shape and moves toward the adhesion site (movie S1 and Fig. 1D). Directed advance of the C-domain toward the adhesion site was accompanied by dramatic reorganization of the underlying actin filament structure (Fig. 1E) including 1) disappearance of radial actin bundles from the target interaction corridor, 2) accumulation of a ring of actin at the bead adhesion site (blue arrow), and 3) dramatically increased intensity of actin arcs (compare yellow arrow heads Fig. 1B, E, respectively). Actin arcs also appeared to constrain or corral C-domain organelles before and during the targeted growth response (cf. yellow arrowheads and dashed lines in Fig. 1A-B and 1D-E).

Assessment of actin flow vectors (Fig. 1F, movie S2) demonstrated that P-domain flow was strongly attenuated within the growth corridor confirming the interpretation of previous indirect measurements (Lin and Forscher, 1995; Suter et al., 1998). Significantly, retrograde flow attenuation was also correlated with rapid restructuring of the P-domain actin filament network in the interaction corridor (Fig. 1E) as well as advance of the C-domain (Fig. 1D). In contrast, actin flow rates and structure in regions adjacent to the growth corridor were largely unchanged (Fig. 1A, C vs 1D, F; (Lin and Forscher, 1995; Suter et al., 1998). Interestingly, during the course of a target interaction actin arcs became strikingly more prominent, especially along the sides of the growth cone. During the target interaction, actin arcs became progressively aligned with the direction of growth, and appeared to define the boundary of the new T-zone (movie S1). The mechanistic implications of these novel structural dynamics are considered below.

Slowing of Retrograde Actin Flow Precedes Formation of Growth Corridor

When growth cones are not interacting with a target substrate, a steady state exists where the rate of assembly at the leading edge is matched by the rates of retrograde actin flow and radial actin bundle recycling in the T-zone (Medeiros et al., 2006; Schaefer et al., 2002). Under these conditions the T-zone/C-domain boundary is relatively stationary and there is no net advance (engorgement) of organelles into the periphery (Fig. 2A, yellow lines). Later, retrograde flow begins to slow (green line, ~ 120 sec) and C-domain advance can be detected ~ 20 sec later in this interaction (Fig. 2A, cf. yellow vs white lines). By the 200 sec time point, there is clearly

an alteration of actin filament structure in the growth corridor (red arrow heads) that appeared to precede the advance of C-domain organelles towards the bead.

What could account for the observed C-domain advance toward the target substrate? To address this question we recorded actin filament dynamics and calculated corresponding actin flow fields in the entire growth cone and within the target interaction axis (*inset*: white rectangle, Fig. 2B-C, movies S2-S3). About 350 sec after bead application, retrograde actin flow in the P-domain and T-zone slowed markedly and eventually came to a near complete halt in the T-zone in a ~40 sec interval (Fig. 2C, dashed outline) that preceded rapid T-zone advance (Fig. 2B, red line). Note that a sharp boundary was maintained between the shrinking P-domain and the advancing C-domain in the growth corridor (red line, 430-510 sec). These observations are consistent with actin filament recycling (Medeiros et al., 2006) continuing in the target interaction axis when retrograde flow rates slow or stop. Continued actin recycling in the face of reduced retrograde flow could then promote forward displacement of the T-zone and C-domain specifically in the target interaction axis.

We also noted that as actin flow attenuation developed in the P-domain and T-zone, flow in more central regions typically *reversed* direction, with clear evidence of anterograde movement present by the end of this sequence (Fig 2C). The flow vector algorithm likely detects movement of actin arcs, actin bundles, and possibly an F-actin component associated with internal membrane organelles in the C-domain (AWS, unpublished observations). To further investigate kinetic coupling between P and C-domains, actin flow vectors were simultaneously generated near the bead and in a more proximal region (*inset*, red and green areas of interest, respectively). Resulting average speed and direction are plotted over time in (Fig 2D). Remarkably, all of the detected F-actin features simultaneously reversed direction and moved in an anterograde direction at the onset of C-domain advance (Fig 2D, compare blue lines). These experiments revealed the presence of novel coordinated long range actin interactions that strongly suggest physical connectivity between the bead adhesion site and proximal regions of the C-domain >20 μm away.

Actin Filament Restructuring Precedes C-domain MT Advance

What factors influence trajectories of MT advance within the growth axis? Recent evidence suggests MT interactions with actin filament structures can guide MT assembly, affect MT assembly rates, and promote MT translocation (Rodriguez et al., 2003; Schaefer et al., 2002). Indeed, earlier we hypothesized that MT interactions with peripheral retrograde actin flow acts as a barrier which limits MT density in the P-domain (Schaefer et al., 2002), thus, we investigated the timing of actin filament restructuring and MT advance during evoked growth responses using triple channel DIC/MT/actin filament recordings. The time montage in Fig. 3 shows the distribution of organelles, actin filaments and MTs at the target site during the course of a growth event (see also movie S4). The leading edge boundary is outlined by a white hatched line in the DIC channel. The advancing C-domain boundary is marked with a yellow hatched line. In this example, the leading edge remains attached to the poly-L-lysine substrate and grows beyond the adhesion site as the C-domain advances. Radial actin bundles are clearly present in the P-domain at the start of the sequence (Fig. 3, column A). These actin bundles likely promote efficient MT interrogation of the bead adhesion site during the latency phase (Suter et al., 2004). Note the presence of a dynamic MT (green arrow head) under the target bead before C-domain advance Fig. 3B (movie S4). Significantly, invasion of C-domain MTs and organelles occurs only after formation of the corridor depleted of F-actin (Fig. 3C, red hatched line). Single dynamic MTs continue to explore beyond the main mass of MTs as the C-domain advances and the P-domain extends beyond the adhesion site (Fig. 3D, green arrow heads). In summary, advance of the bulk of MTs comprising the C-domain follows formation

of a corridor leading to the target site that is depleted of F-actin -consistent with removal of a structural actin barrier to C-domain advance.

C-domain Advance Results from both MT Assembly and Sliding

MTs densely populate the C-domain and their reorganization contributes to the morphological changes observed during the growth response (Suter et al., 1998); however, the mechanism(s) of MT advance during substrate evoked growth are unknown. To address this issue, neurons were injected with low levels of alexa-594 tubulin to monitor MT dynamics by FSM during apCAM bead evoked growth responses. Corresponding structural changes were observed with DIC as above. Under control conditions, MTs are mainly restricted to the C-domain. However, a highly dynamic population of MTs constantly “explore” the P-domain by transient bursts of polymerization guided by MT association with radial actin bundles (Schaefer et al., 2002). Growth cone structure and MT distribution during the latency phase and after completion of an apCAM target interaction are illustrated in Fig. 4A-B, respectively. During the course of the interaction, C-domain organelles and underlying MTs (4B top, bottom, respectively) moved toward the restrained bead (movie S5). To quantify structural (DIC) and MT dynamics during this interaction the kymograph shown in Fig. 4C was generated using a sampling region spanning the target interaction axis between the C-domain and past the leading edge (4A, yellow line). Deep excursions of individual highly dynamic MTs into the P-domain were observed during the latency period (4C, green arrowheads). These transient events represent stochastic, spatially unbiased MT sampling of the P-domain and do not result in significant MT accumulation or MT “docking” at the bead site during the latency period (movies S4 and S5). These MT “explorations” are driven primarily by plus-end MT assembly and are necessary to support signaling involved in apCAM target recognition (Suter et al., 2004).

During the growth phase, C-domain organelles and MTs advanced in parallel toward the target site (Fig. 4B). Advance of the C-domain organelle boundary and MTs are indicated by yellow lines in the kymograph (Fig. 4C). The rate of MT (or organelle) advance was $\sim 3.7 \mu\text{m min}^{-1}$ which is similar to previous values obtained using this assay (Suter et al., 1998). Note deflection of the restraining needle in the kymograph (red arrow) as tension develops between the target substrate and growth cone.

The high density of MTs entering the growth corridor combined with the short spatial-temporal window of C-domain advance prevented a robust statistical analysis of MT polymerization rates; however, analysis of unambiguous single MTs in the target interaction corridor suggests advance of the C-domain results from a combination of both MT sliding and polymerization. Fig 4D is a time-lapse montage illustrating C-domain advance and the underlying behavior of MTs advancing as the growth corridor forms. Fig. 4E-F shows the behavior of individual MTs denoted (e) and (f) in Fig. 4D. These C-domain MTs typically exhibited slow but persistent growth (arrows point to MT plus-ends) when compared to the highly dynamic MTs normally present in the P-domain under control conditions (Schaefer et al., 2002). Analysis of internal speckle displacements illustrates simultaneous MT translocation towards the adhesion site (Fig. 4E-F yellow lines; translocation at 4.7 and $2.1 \mu\text{m min}^{-1}$, respectively). Looped MTs within the target interaction corridor were also observed to straighten over time (Fig. 4E, yellow arrowheads; movie S5). Thus, sliding (translocation) and polymerization both appear to contribute to the advance of MTs that underlies C-domain engorgement during evoked growth responses.

Actomyosin II Arcs Shape C-Domain Advance

C-domain advance is accompanied by increased tension as traction force develops between a restrained bead substrate and the growth cone (Suter et al., 1998). However, the cytoskeletal effectors responsible for tension generation are unknown. Actin arcs are myosin II dependent

contractile structures that form in the T-zone from condensation of the peripheral actin networks (Schaefer et al., 2002) and play a key role in actin bundle turnover and recycling in this region (Medeiros et al., 2006). Although actin arcs have been implicated as an effector in Rho-mediated growth cone retraction (Zhang et al., 2003), their possible role in substrate-dependent growth has not been characterized.

Interestingly, when organelles engorged the periphery and the C-domain advanced toward the adhesion site (dashed line, Fig. 5A), actin arcs on the sides of the C-domain become strikingly more robust and straightened (Fig. 5B; compare yellow arrows at 30 sec vs 650 sec, movie S6). Also, the distal ends of actin arcs appeared to be embedded in the actin filament network near the restrained bead by the end of growth phase (Fig. 5B, red arrowheads). An intense ring of F-actin was also typically present around the bead binding site at this point (Fig. 5B, 650 sec).

To investigate kinetic coupling between the actin arc system and the adhesion site, flow vectors were assessed for movements detected on lateral aspects of the growth cone (Fig. 5C). This analysis revealed slow, generally centripetal actin arc movements during the latency period (Fig. 5C, 30 sec) consistent with observations of un-stimulated growth cones (Supplemental Figs 1 and 2) (Schaefer et al., 2002). However, actin arcs rapidly reoriented their trajectories and began moving toward the target site during the growth phase (Fig. 5C, last panel). The abrupt change in arc direction is illustrated in Fig. 5D where average actin arc trajectories and speeds sampled in the area indicated (Fig. 5C, dotted line) are plotted over time. Upon entering the growth phase, arc trajectories reoriented counterclockwise ~ 90 degrees and net arc movement was now toward the restrained bead target (movie S7). As arcs straightened, their speed also slowed to about 1/3 of pre-interaction rates (Fig. 5D, purple line). Taken together, these observations strongly suggest arcs mediate a progressive build-up of tension and the long range transduction of forces (in this case the area of interest was ~ 20 μm from the adhesion site) over the course of the growth response.

We recently reported that the myosin II dependent actin arc contractility exerts shear force that promotes the severing of filopodium roots in the T-zone (Medeiros et al., 2006). Fig. 5E shows a region of interest from 5A (white box) analyzed at higher magnification. Inspection of the flow fields (Fig. 5E, right column) shows initial centripetal (i.e. lateral) movement of actin arcs into the C-domain during the latency period and reorientation of arc vectors towards the adhesion site during the growth phase. The abrupt radial actin bundle terminations and clear T-zone boundary (Fig. 5E, yellow line) along the lateral aspects of the growth cone likely results from shear imposed by actin arcs positioned orthogonal to radial actin bundles arriving by retrograde actin flow (see movie S7). Note the sharpness of the T-zone boundary is maintained even as its position shifts over time (yellow line).

To further investigate substrate-to-arc connectivity, beads were rapidly displaced and corresponding structural (DIC) and actin filament movements recorded during the interaction (movie S8). Arcs immediately straightened and extended when bead targets were pulled forward indicating mechanical continuity. Conversely, when the bead was released, both bead and actin arcs moved into the C-domain at similar rates resulting in elimination of the interaction corridor. Actin arcs rapidly resumed their typical curved morphology surrounding the C-domain after bead release. More detailed biophysical analysis of these effects was complicated by frequent breakage and reformation of actin bundles in response to applied force; however, mechanical connectivity between restrained beads, actin arcs and the C-domain is evident.

Actin Arcs Regulate MT behavior on the sides of C-domain

MTs associated with actin arcs exhibit low catastrophe frequencies that promote their efficient growth in contrast to peripheral MTs which are dynamically unstable. Actin arcs also function as a transport system that move MTs into the C-domain on the sides of the growth cone (Schaefer et al., 2002). Given the above, increased actin arc prominence on the sides of growth cones during interactions (e.g. Fig. 5B) suggested actin arcs could be regulating MT behavior on the sides of the growth cone during target interactions.

Fig. 6A shows representative actin and MT labeling patterns acquired from one side of a growth cone (*inset*, area of interest (a)) during a target interaction. Note similar orientation of actin arcs and MTs (*yellow arrows*). Fig. 6B is a flow field time series captured from area of interest (b) as the growth cone transitioned into the acute growth phase (see movie S9). Throughout the latency period, both actin filaments and MTs in the T-zone exhibited centripetal movement into the C-domain, consistent with previous findings (Schaefer et al., 2002). In contrast, as the target interaction entered the growth phase, actin filament and MT vectors both suddenly turned $\sim 90^\circ$ counterclockwise (Fig. 6B and plotted in Fig. 6C) and movement was now toward the adhesion site. These observations show that actin arc and MT movements are highly coordinated.

Average MTs speeds tended to be slower than the surrounding actin filaments (Fig. 6B, vectors) prompting us to characterize the degree of molecular coupling between F-actin and MTs during the growth response. To address this, direction coupling scores (DCS) and velocity magnitude coupling scores (VMCS) were calculated (Fig. 6D) (Hu et al., 2007). The observed average DCS ~ 0.6 and VMCS ~ 0.5 scores (Fig. 6D, blue circles and purple squares) demonstrated a significant degree of coupling between the actin arcs and MTs which accounts for the coordinated turning of MT and arc movements during the growth phase. Interestingly, the two polymer systems do not appear to be perfectly coupled (scores < 1) suggesting their interactions could be dynamically regulated up or down. In summary, this detailed kinematic analysis strongly supports the hypothesis that actin arcs are coordinating MT movements on the sides of the growth cone during episodes of evoked growth.

Rho Kinase Activity Regulates C-domain Advance and MT Consolidation

Rho Kinase activity is known to regulate actin arc contractility and stability, and also to constrain MT distribution in the C-domain (Zhang et al., 2003). Interestingly, Rho Kinase inhibition halted actin arc movement and associated MT transport in the growth cone T-zone and C-domain (Zhang et al., 2003). Given the prominence of actin arcs in the late phase of evoked growth responses (Fig. 5B) we investigated how altering Rho Kinase and corresponding arc contractility might affect evoked growth responses.

First, control growth responses were evoked with apCAM substrates. Note the focused bullet-like shape of the C-domain 984 sec after apCAM bead placement (Fig. 7A, hatched white line marks C-domain boundary). The same growth cone was then treated with the Rho Kinase inhibitor Y27632 and a second growth episode initiated. Interestingly, after Rho Kinase inhibition the C-domain advanced to the adhesion site in less than half the time (444 sec); however, the proximal C-domain was $\sim 33\%$ broader than the control (Fig. 7B, black lines). Statistical analysis showed that the decrease in the latency phase after Rho Kinase inhibition was significant and the effects were reversible (Fig. 7C). Interestingly, once evoked growth started, the rate of C-domain advance did not depend on Rho Kinase activity (control 4.4 ± 1.1 versus 4.3 ± 0.8 SEM μmmin^{-1} ; $n=7$). These observations suggested that Rho Kinase is regulating a barrier to C-domain advance but not the advance process itself.

To address underlying mechanism, we compared actin dynamics under control conditions vs. in the presence of Rho Kinase inhibitor. Focal actin cup assembly and corridor formation was observed by the end of the growth phase in both controls and after drug treatment (blue circles, Fig. 7D and 7E respectively). Actin arcs were clearly visible proximal to the adhesion site under control conditions (Fig. 7D, blue box). In contrast, actin arc density was greatly reduced in the presence of Rho Kinase inhibitor. This was especially evident on the sides of the growth cone (Fig. 7E, blue box). These results are consistent with our earlier report that Rho Kinase inhibition decreases actin arc lifetimes and inhibits arc contractility (Zhang et al., 2003). Inspection of control actin flow fields in this region revealed a generally centripetal actin flow pattern during the latency phase (Fig. 7F, Control, left column) which turned strongly toward the adhesion site during the growth phase (Control, right column) similar to Fig. 6. In contrast, actin filament movements were much less coherent after Rho Kinase inhibition during both latency and growth phases (Rho Kinase inhibition, left and right columns, respectively). Moreover, coordinated turning of flow vectors toward the target site during the growth phase was no longer evident.

To further characterize actin responses, the directional coherence (Hu et al., 2007) of actin filament movement over time was assessed for regions of interest in (D) and (E) and plotted in Fig. 7G. Actin filament movements were highly coherent, i.e. speckles tended to move in tandem in the same direction, throughout the control interaction (~0.9 out of 1.0); in contrast, directional coherence was reduced (~0.5) in the presence of Rho Kinase inhibitor.

Actin arc presence during the growth response also had a dramatic effect on MT organization in the C-domain. Under control conditions, the majority of C-domain MTs were bundled into a single growth axis directed toward the adhesion site (Fig. 7H, white arrow, left panel, also Supp Fig. 3). In contrast, after Rho Kinase inhibition, although some MTs reached the adhesion site (Fig. 7H, white arrow, right panel), many MTs remained splayed out in the C-domain and failed to consolidate into a unitary axis of growth.

Inspection of F-actin in the control revealed the presence of actin arcs surrounding the growth corridor under control conditions (Fig. 7I, left panel, yellow arrows), whereas, actin arcs were essentially absent in the same region with Rho Kinase inhibition (Fig. 7I, right panel). Although we can not rule out other (i.e., arc-independent) effects of Rho Kinase, these results suggest: 1) actin arcs form a dynamic barrier around the C-domain that regulates the rate of bulk MT advance; 2) arcs capture MTs on the sides of the growth cone and actively transport them into the C-domain. The latter process appears to play a key role in establishing a single axis of MT advance during periods of evoked growth. These novel Rho Kinase dependent actin arc functions will be considered further below.

Discussion

This study represents the first direct analysis of the cytoskeletal events underlying substrate dependent neuronal growth. Actin recycling, actin remodeling, and actomyosin II arc contractility emerge as key processes involved in regulation of C-domain advance and underlying MT behavior. We discuss the sequential steps in a substrate evoked growth cycle below in the context of the model shown in Fig. 8.

Adhesion & Signaling during the Latency Period

After bead placement, clustering of apCAM is followed by assembly of a cup-like actin filament structure around the restrained bead (Figs. 1 and 8A) that appears to act as a scaffold for signaling proteins involved in regulation of apCAM adhesion (Suter et al., 1998; Suter and Forscher, 2001). Initially, actin filament flow is unchanged (Fig. 1-2) and mechanical tension between the bead and growth cone is low. During this period, actin filaments and MTs interact

in a dynamic steady state that maintains the position of the C/P-domain boundary (Schaefer et al., 2002). Retrograde actin flow constantly moves actin filaments assembled at the leading edge into the T-zone where local actin network contraction occurs, and radial filopodial actin bundles embedded in the contracting network are severed and recycled by a myosin II facilitated process (Forscher and Smith, 1988; Lin et al., 1996; Medeiros et al., 2006). MT association with retrograde moving radial actin bundles also results in MT transport out of the P-domain and into the T-zone where MT buckling, breakage, and minus-end catastrophes typically occur. Thus, peripheral actin filament dynamics play a role in regulating MT advance and MT turnover (Schaefer et al., 2002).

During the latency phase MTs continue to stochastically explore the P-domain by bursts of assembly that appear to be guided by radial actin bundles (Schaefer et al., 2002). This ongoing process appears to provide an efficient mechanism for MT sampling of the P-domain (Kirschner and Mitchison, 1986) related to signal transduction. Indeed, dynamic MTs are required for persistent growth and turning at inhibitory borders (Challacombe et al., 1997; Tanaka et al., 1995; Tanaka and Kirschner, 1995; Williamson et al., 1996), recruitment of active src family kinase to apCAM bead binding sites, and development of adhesion dependent traction forces in *Aplysia* growth cones (Suter et al., 2004). Here, we report that during the latency period, MTs continued to interrogate the entire P-domain and did not dock or accumulate at the adhesion site (Figs. 3, 4 and 8A) consistent with a signaling rather than a structural role for peripheral MTs in substrate evoked growth.

What factors maintain the C-domain position during the latency phase? It has long been known that acute removal of peripheral actin networks after cytochalasin treatment leads to C-domain advance, suggesting MTs are normally restrained by a barrier associated with the presence of actin filament networks (Forscher and Smith, 1988) and several lines of evidence suggest that C-domain MTs are actually under compressive restraint (Ahmad et al., 2000; Dennerll et al., 1988; Joshi et al., 1985).

Actin arcs may functionally contribute to the barrier since they constantly capture MTs and transport them into the C-domain. This process is particularly evident on the sides of the growth cone (Schaefer et al., 2002). Interestingly, Rho Kinase inhibition resulted in a marked decrease in the latency phase (Fig. 7) –i.e. growth responses occurred with less delay after bead application. This finding is consistent with actomyosin II arc contractility acting as a dynamic barrier or restraint to C-domain organelle and MT advance during the latency phase (Fig. 8A). What signalling pathways might regulate this barrier? Src family kinases are one candidate since src activity is required for apCAM evoked growth (Suter et al., 2004), and, in related studies, src has been implicated in cyclical inhibition and reactivation of Rho during integrin mediated motility (DeMali et al., 2003). Adhesion site formation and turnover is regulated by a src-FAK complex (Brunton et al., 2004), and FAK mediated phosphorylation is required for integrin dependent adhesion in neurons (Robles and Gomez, 2006). Characterization of src effectors in regulating apCAM dependent adhesion will be interesting questions for future studies.

Corridor Formation during the Growth Phase

Progressive coupling of the adhesion site to the underlying actin cytoskeleton is associated with slowing of retrograde flow in the target interaction axis (Fig. 1-3, Suter et al., 1998). Flow attenuation is immediately followed by a cascade of events that include: 1) restructuring of actin to form a growth corridor, 2) MT extension by both translocation and polymerization, and 3) P-domain advance past the adhesion site (Fig 8B).

Growth corridor formation could simply evolve from continued actin bundle recycling in the T-zone in the face of attenuated retrograde flow rates which would result in forward

displacement of the T-zone (e.g. Fig. 2B) followed by directed C-domain advance (Fig. 1-2). This scenario assumes that when retrograde flow slows down, a forward migration of the actin bundle recycling zone occurs. Image sequences such as that shown in Fig. 2B are consistent with this scheme; however, an alternate, but not exclusive, possibility is corridor formation by *de novo* activation of a localized process that disrupts existing actin networks.

What could this be? Accelerated actin filament shrinkage due to faster disassembly and/or severing rates could move the T-zone forward. Alternatively, actin bundles could be destabilized by inactivation of an actin bundling protein such as α -actinin or fascin. To date, the mechanism(s) of actin filament recycling in the growth cone are incompletely understood although severing proteins such as cofilin and/or gelsolin are obvious candidates here (Lu et al., 1997; Meberg and Bamberg, 2000; Meberg et al., 1998). Quantification of actin turnover kinetics combined with perturbation of candidate proteins will be required to further address the mechanism of corridor formation (Ponti et al., 2005; Vallotton et al., 2004).

A Novel Role for Rho Kinase and Actomyosin Tension in Neurite Shaft Consolidation

Late in the growth phase, stronger traction forces appear to be generated (Suter et al., 1998) and long range transfer of tension along the neurite shaft can occur (Bray, 1979; Lamoureux et al., 1989). Vector field analysis and Rho Kinase inhibition experiments are consistent with actin arcs generating tension between the C-domain and remote distal sites of adhesion (Figs. 5-7). What specific role(s) could arc contractility play in neurite advance? As the growth responses progressed, actin arcs became more prominent on the lateral aspects of the growth cone where they associate with MTs and orient toward the adhesion site (Figs. 1,5 and 8C). Previously we showed that MTs associated with actin arcs grow very efficiently as a result of low catastrophe frequencies (Schaefer et al., 2002; Zhang et al., 2003, Fig.6). Taken together these results suggest actin arcs may help guide MT growth toward adhesion sites. An analogous situation may exist in fibroblasts where MT targeting to focal adhesions appears to be by association with actin filament bundles (Kaverina et al., 1999; Krylyshkina et al., 2003).

Tension increases observed between the growth cone and the adhesion site (Suter et al., 1998); Fig. 8C, red arrows) may be mediated by actin arcs (Fig. 5-7, Supp Fig. 3). This idea is consistent with findings of myosin II localized to actin arc-like structures in the T-zone of vertebrate growth cones (Bridgman, 2002; Rochlin et al., 1995) and that growth cones with impaired myosin IIb function generated less traction force (Bridgman et al., 2001) and had decreased neurite outgrowth rates (Wylie et al., 1998).

During growth responses, actin arcs also interacted strongly with MTs on the sides of the advancing C-domain and their respective movements are coordinated (Fig. 6). In a separate study, we provide evidence that MT association with actin arcs results in MT transport into the C-domain. As a result, MTs are compressed into bundles in the growth cone neck and this process is myosin II dependent (Burnette et al., unpublished observations). MT compression may facilitate crosslinking by MAPs (MT associated proteins) known to be necessary for stabilization and consolidation of a new segment of the axon shaft (Bielas et al., 2007). Interestingly, in the current study, extending MTs exhibited excessive splaying and no longer formed a unified axis of growth after Rho Kinase inhibition (Fig. 7, Supp Fig. 3). Given that Rho Kinase regulates myosin II contractility, actin arc motility and arc stability (Zhang et al., 2003), we suspect that inefficient MT transport may explain the effects of Rho Kinase inhibition on MT distribution seen in Fig. 7.

Physiological Implications

Previous studies have shown that myosin II activity is required for turning at inhibitory borders (Turney and Bridgman, 2005) or towards NGF coated beads (Loudon et al., 2006). The current

study suggests that actin arc contractility could play a role in growth cone turning by maintaining a unified axis of advance as the C-domain changes direction. In another functional context, Rho→Rho Kinase signaling has been implicated in axon repulsion at least partly through modulation of myosin II activity (for review see: (Schmandke et al., 2007). This has spurred clinical interest in use of Rho and/or Rho Kinase inhibitors as nerve regeneration agents (for review, (Mueller et al., 2005). Interestingly, Rho Kinase inhibitors reduce the effectiveness of attractive cues and result in aberrant neurite trajectories (Causeret et al., 2004). The current study suggests that Rho→Rho Kinase inhibition strategies could present a “double edged therapeutic sword” -promoting permissive growth by reducing a barrier to C-domain advance while at the same time reducing directional control as a result of inefficient MT transport and bundling.

Materials and Methods

Cell Culture and Target Interaction Assay

Aplysia Bag cell neurons were cultured on poly-L-lysine coated cover-slips in L15 medium (Life Technologies, Frederick, MD) with artificial seawater (ASW) as previously described (Forscher et al., 1987). The assay was performed on growth cones as previously described (Suter et al., 1998). Prior to the experiment, cells were incubated for one hour with 0.025% fetal bovine serum and during the experiments phenol-free medium was supplemented with 2-4 mg/ml BSA to block nonspecific bead binding. The bead substrates were prepared by coating 5 μ m silica Ni-NTA beads (Micromod, Germany) with purified recombinant apCAM (Suter et al., 2004). Cell injection and subsequent fluorescent imaging decreased the likelihood of bead substrate interactions. Cytoskeletal dynamics were only analyzed for robust growth responses as monitored in the DIC channel.

Immunocytochemistry

Immunofluorescence as previously described (Lin and Forscher, 1993). Alexa-Fluor 594 conjugated phalloidin (Molecular Probes) was used for actin filament labeling. Cells were stained for one hour to visualize fine actin structures. For MT labeling, mouse mAb clone B-5-1-2 (Sigma-Aldrich) was used with Alexa-Fluor 488 conjugated goat anti-mouse secondary antibody (Molecular Probes Inc.). Images acquired using a Nikon Eclipse TE300 microscope with a Coolsnap HQ cooled CCD camera (Roper Scientific) and Metamorph software (Universal Imaging).

Rho Kinase Inhibition Experiments

Cells were incubated with medium supplemented 10 μ m lysophosphatidic acid (LPA) for 30 minutes before control latency periods were measured to establish a Rho signaling baseline (Zhang et al., 2003). Subsequently, media with 20 μ m Y-27632 and 10 μ m LPA was added to the cell chamber for 30 minutes, and the targeted growth assay was conducted on the same growth cone. The Rho Kinase inhibitor was washed out by incubating cells for 30 min in medium with 10 μ m LPA before the growth assay was repeated. Latency times were calculated, normalized against control times and averaged. Data are expressed as mean \pm SEM. Statistical analysis was performed with two-tailed paired t-test.

Multimode FSM

Microinjection protocol as described previously (Lin and Forscher, 1995). For actin dynamics, neurons were injected with Alexa-Fluor 594 or Alexa-Fluor 488 phalloidin (needle concentration 20 μ M, Molecular Probes Inc.). For MT dynamics, neurons were injected with 1 mg/ml Alexa-Fluor 594 labeled tubulin (Molecular Probes Inc.). Reagent or vehicle solution injections were typically ~10% of cell volume. After microinjection, cells were incubated in

L15/ASW one hour before imaging. Multimode time-lapse microscopy was as previously described. Briefly, total internal reflection fluorescence (TIRF) microscopy was performed on a Nikon Eclipse 2000 multimode TIRF microscope prototype. Metamorph control software (Universal Imaging, West Chester PA) was used for instrument control. Images were acquired with a CoolSnapHQ CCD camera using 10s or 12s intervals and 300-700 ms integration times for fluorescent probes and 50 ms for DIC. Pixel size =107 nm.

Image Processing and Analysis

Raw Tiff data was used for flow tracking analysis. Time-lapse movie sequences were converted into image montages for figure presentation. For presentation, the MT fluorescent images were processed with the following spatial filters: unsharp mask, low pass, laplace edge enhancement, and a final low pass using Metamorph Software. For F-actin, unsharp mask and low pass spatial filters were used to enhance contrast. A threshold look up table was applied to MT images before combining with the DIC image to clear low level background noise for DIC-fluorescent overlays. Images were sized in Photoshop, converted to Jpeg format, and figures organized in Canvas.

Flow Tracking and Analysis

An adaptive multi-frame correlation approach was used as described previously (Ji and Danuser, 2005) to track the motion of fluorescently labeled F-actin and MTs in the time-lapse image sequences. To track random features of unknown shape and contrast in growth cone images, we used a texture-based tracking method that relied on the correlation between signals in consecutive frames to estimate the translocation of small windows, referred to as templates, between the two time points. Due to continuous assembly and disassembly of F-actin and MTs and because of imaging noise, the signal in one template was sometimes too unstable for the accumulation of a cross-correlation function with a unique maximum reflecting the displacement of the template between two frames. To address this issue, our method integrates the cross-correlation functions of the same template region over multiple consecutive frame pairs, with the assumption the flow speed and direction within a single template are locally stationary, i.e. do not change over the sampling interval. This permitted flow field tracking with high spatial resolution and moderate but adequate time resolution. Flow fields were calculated for sequences of overlapping 3 frame windows with a time step of one frame (time-lapse images were acquired at 10 or 12 second intervals). Thus, flow fields presented here indicate the velocity of features averaged over 30s to 36s. Flow fields were overlaid on the raw image and scaled by a factor 3.

In addition to time integration, our program can adaptively adjust template size and resulting spatial resolution depending on local image contrast. Flow measurements in image regions with high contrast can afford smaller templates while image regions with low contrast require larger templates. The user defines the bounds of achievable spatial resolution by specifying minimum and maximum template sizes. In this study we chose 11 pixels (~ 1 μ m) as the lower template boundary corresponding to an area ~four times that of a diffraction-limited spot. Upper bounds were 21 pixels (~ 2 μ m) for F-actin and 41 pixels (~ 4 μ m) for MT.

A detailed description of the coupling analysis was described in (Hu et al., 2007). The coherency score was calculated by taking all the normalized vectors in a sample box of 25 \times 25 pixels ($1/N\sum V_i/|V_i|, |V_i V_i|$, normalized unit vector, N the number of vectors in the box) and calculating the magnitude of the vector mean. If the flow vectors in the box all point to the same direction, the score is 1. Otherwise if their directions are random, it is close to zero. The average score of all sample boxes that cover the whole ROI is graphed. Velocity Magnitude Coupling Score (VMCS) measures the coupling of velocity magnitudes of two flow fields (actin and MT) along a common axis excluding random fluctuations. Note it is different from

a speed ratio. However, when there is no random fluctuation and the two flow fields are perfectly aligned, it is the same as a speed ratio. Direction Correlation Score (DCS) is defined as the $\cos\theta$ of the angle between paired (actin and MT) flow vectors.

Supplementary Material

Refer to Web version on PubMed Central for supplementary material.

Acknowledgments

The authors would like to thank members of the Forscher lab for helpful comments and discussion. We thank Dylan Burnette for generating the data used in Supplemental Figure 1. We thank Drs. Mark Mooseker and Tony Koleske for critical reading and their insightful comments. This work was supported by NIH grant RO1-NS28695 to P.F. and the Nikon Partners-in-Research Program

References

- Ahmad FJ, Hughey J, Wittmann T, Hyman A, Greaser M, Baas PW. Motor proteins regulate force interactions between microtubules and microfilaments in the axon. *Nature cell biology* 2000;2:276–280.
- Bentley D, O'Connor TP. Cytoskeletal events in growth cone steering. *Curr Opin Neurobiol* 1994;4:43–48. [PubMed: 8173324]
- Bentley D, Toroian-Raymond A. Disoriented pathfinding by pioneer neurone growth cones deprived of filopodia by cytochalasin treatment. *Nature* 1986;323:712–715. [PubMed: 3773996]
- Bielas SL, Serneo FF, Chechlacz M, Deerinck TJ, Perkins GA, Allen PB, Ellisman MH, Gleeson JG. Spinophilin facilitates dephosphorylation of doublecortin by PP1 to mediate microtubule bundling at the axonal wrist. *Cell* 2007;129:579–591. [PubMed: 17482550]
- Bray D. Mechanical tension produced by nerve cells in tissue culture. *Journal of cell science* 1979;37:391–410. [PubMed: 479327]
- Bridgman PC. Growth cones contain myosin II bipolar filament arrays. *Cell Motil Cytoskeleton* 2002;52:91–96. [PubMed: 12112151]
- Bridgman PC, Dave S, Asnes CF, Tullio AN, Adelstein RS. Myosin IIB is required for growth cone motility. *J Neurosci* 2001;21:6159–6169. [PubMed: 11487639]
- Brunton VG, MacPherson IR, Frame MC. Cell adhesion receptors, tyrosine kinases and actin modulators: a complex three-way circuitry. *Biochimica et biophysica acta* 2004;1692:121–144. [PubMed: 15246683]
- Buck KB, Zheng JQ. Growth cone turning induced by direct local modification of microtubule dynamics. *J Neurosci* 2002;22:9358–9367. [PubMed: 12417661]
- Causeret F, Hidalgo-Sanchez M, Fort P, Backer S, Popoff MR, Gauthier-Rouviere C, Bloch-Gallego E. Distinct roles of Rac1/Cdc42 and Rho/Rock for axon outgrowth and nucleokinesis of precerebellar neurons toward netrin 1. *Development (Cambridge, England)* 2004;131:2841–2852.
- Challacombe JF, Snow DM, Letourneau PC. Actin filament bundles are required for microtubule reorientation during growth cone turning to avoid an inhibitory guidance cue. *Journal of cell science* 1996;109(Pt 8):2031–2040. [PubMed: 8856499]
- Challacombe JF, Snow DM, Letourneau PC. Dynamic microtubule ends are required for growth cone turning to avoid an inhibitory guidance cue. *J Neurosci* 1997;17:3085–3095. [PubMed: 9096143]
- Danuser G, Waterman-Storer CM. Quantitative fluorescent speckle microscopy of cytoskeleton dynamics. *Annu Rev Biophys Biomol Struct* 2006;35:361–387. [PubMed: 16689641]
- De La Cruz EM, Pollard TD. Kinetics and thermodynamics of phalloidin binding to actin filaments from three divergent species. *Biochemistry* 1996;35:14054–14061. [PubMed: 8916890]
- DeMali KA, Wennerberg K, Burridge K. Integrin signaling to the actin cytoskeleton. *Curr Opin Cell Biol* 2003;15:572–582. [PubMed: 14519392]

- Dennerll TJ, Joshi HC, Steel VL, Buxbaum RE, Heidemann SR. Tension and compression in the cytoskeleton of PC-12 neurites. II: Quantitative measurements. *The Journal of cell biology* 1988;107:665–674. [PubMed: 3417767]
- Dent EW, Gertler FB. Cytoskeletal dynamics and transport in growth cone motility and axon guidance. *Neuron* 2003;40:209–227. [PubMed: 14556705]
- Forscher P, Kaczmarek LK, Buchanan JA, Smith SJ. Cyclic AMP induces changes in distribution and transport of organelles within growth cones of Aplysia bag cell neurons. *J Neurosci* 1987;7:3600–3611. [PubMed: 2824715]
- Forscher P, Smith SJ. Actions of cytochalasins on the organization of actin filaments and microtubules in a neuronal growth cone. *The Journal of cell biology* 1988;107:1505–1516. [PubMed: 3170637]
- Gallo G, Letourneau PC. Regulation of growth cone actin filaments by guidance cues. *J Neurobiol* 2004;58:92–102. [PubMed: 14598373]
- Goldberg DJ, Burmeister DW. Stages in axon formation: observations of growth of Aplysia axons in culture using video-enhanced contrast-differential interference contrast microscopy. *The Journal of cell biology* 1986;103:1921–1931. [PubMed: 3782290]
- Guan KL, Rao Y. Signalling mechanisms mediating neuronal responses to guidance cues. *Nat Rev Neurosci* 2003;4:941–956. [PubMed: 14682358]
- Hu K, Ji L, Applegate KT, Danuser G, Waterman-Storer CM. Differential transmission of actin motion within focal adhesions. *Science* 2007;315:111–115. [PubMed: 17204653]
- Huber AB, Kolodkin AL, Ginty DD, Cloutier JF. Signaling at the growth cone: ligand-receptor complexes and the control of axon growth and guidance. *Annu Rev Neurosci* 2003;26:509–563. [PubMed: 12677003]
- Ji L, Danuser G. Tracking quasi-stationary flow of weak fluorescent signals by adaptive multi-frame correlation. *J Microsc* 2005;220:150–167. [PubMed: 16363999]
- Joshi HC, Chu D, Buxbaum RE, Heidemann SR. Tension and compression in the cytoskeleton of PC 12 neurites. *The Journal of cell biology* 1985;101:697–705. [PubMed: 2863274]
- Kaverina I, Krylyshkina O, Small JV. Microtubule targeting of substrate contacts promotes their relaxation and dissociation. *The Journal of cell biology* 1999;146:1033–1044. [PubMed: 10477757]
- Kirschner M, Mitchison T. Beyond self-assembly: from microtubules to morphogenesis. *Cell* 1986;45:329–342. [PubMed: 3516413]
- Krylyshkina O, Anderson KI, Kaverina I, Upmann I, Manstein DJ, Small JV, Toomre DK. Nanometer targeting of microtubules to focal adhesions. *The Journal of cell biology* 2003;161:853–859. [PubMed: 12782685]
- Lamoureux P, Buxbaum RE, Heidemann SR. Direct evidence that growth cones pull. *Nature* 1989;340:159–162. [PubMed: 2739738]
- Lee H, Engel U, Rusch J, Scherrer S, Sheard K, Van Vactor D. The microtubule plus end tracking protein Orbit/MAST/CLASP acts downstream of the tyrosine kinase Abl in mediating axon guidance. *Neuron* 2004;42:913–926. [PubMed: 15207236]
- Letourneau PC, Shattuck TA, Ressler AH. “Pull” and “push” in neurite elongation: observations on the effects of different concentrations of cytochalasin B and taxol. *Cell Motil Cytoskeleton* 1987;8:193–209. [PubMed: 2891448]
- Lewis AK, Bridgman PC. Nerve growth cone lamellipodia contain two populations of actin filaments that differ in organization and polarity. *The Journal of cell biology* 1992;119:1219–1243. [PubMed: 1447299]
- Lin CH, Espreafico EM, Mooseker MS, Forscher P. Myosin drives retrograde F-actin flow in neuronal growth cones. *Neuron* 1996;16:769–782. [PubMed: 8607995]
- Lin CH, Forscher P. Cytoskeletal remodeling during growth cone-target interactions. *The Journal of cell biology* 1993;121:1369–1383. [PubMed: 8509456]
- Lin CH, Forscher P. Growth cone advance is inversely proportional to retrograde F-actin flow. *Neuron* 1995;14:763–771. [PubMed: 7536426]
- Lin CH, Thompson CA, Forscher P. Cytoskeletal reorganization underlying growth cone motility. *Curr Opin Neurobiol* 1994;4:640–647. [PubMed: 7849519]

- Loudon RP, Silver LD, Yee HF Jr, Gallo G. RhoA-kinase and myosin II are required for the maintenance of growth cone polarity and guidance by nerve growth factor. *J Neurobiol* 2006;66:847–867. [PubMed: 16673385]
- Lu M, Witke W, Kwiatkowski DJ, Kosik KS. Delayed retraction of filopodia in gelsolin null mice. *The Journal of cell biology* 1997;138:1279–1287. [PubMed: 9298983]
- Marsh L, Letourneau PC. Growth of neurites without filopodial or lamellipodial activity in the presence of cytochalasin B. *The Journal of cell biology* 1984;99:2041–2047. [PubMed: 6389568]
- Meberg PJ, Bamburg JR. Increase in neurite outgrowth mediated by overexpression of actin depolymerizing factor. *J Neurosci* 2000;20:2459–2469. [PubMed: 10729326]
- Meberg PJ, Ono S, Minamide LS, Takahashi M, Bamburg JR. Actin depolymerizing factor and cofilin phosphorylation dynamics: response to signals that regulate neurite extension. *Cell Motil Cytoskeleton* 1998;39:172–190. [PubMed: 9484959]
- Medeiros NA, Burnette DT, Forscher P. Myosin II functions in actin-bundle turnover in neuronal growth cones. *Nature cell biology* 2006;8:216–226.
- Mitchison T, Kirschner M. Dynamic instability of microtubule growth. *Nature* 1984;312:237–242. [PubMed: 6504138]
- Mueller BK, Mack H, Teusch N. Rho kinase, a promising drug target for neurological disorders. *Nat Rev Drug Discov* 2005;4:387–398. [PubMed: 15864268]
- Ponti A, Matov A, Adams M, Gupton S, Waterman-Storer CM, Danuser G. Periodic patterns of actin turnover in lamellipodia and lamellae of migrating epithelial cells analyzed by quantitative Fluorescent Speckle Microscopy. *Biophys J* 2005;89:3456–3469. [PubMed: 16100274]
- Robles E, Gomez TM. Focal adhesion kinase signaling at sites of integrin-mediated adhesion controls axon pathfinding. *Nature neuroscience* 2006;9:1274–1283.
- Rochlin MW, Itoh K, Adelstein RS, Bridgman PC. Localization of myosin II A and B isoforms in cultured neurons. *Journal of cell science* 1995;108(Pt 12):3661–3670. [PubMed: 8719872]
- Rodriguez OC, Schaefer AW, Mandato CA, Forscher P, Bement WM, Waterman-Storer CM. Conserved microtubule-actin interactions in cell movement and morphogenesis. *Nature cell biology* 2003;5:599–609.
- Sabry JH, O'Connor TP, Evans L, Toroian-Raymond A, Kirschner M, Bentley D. Microtubule behavior during guidance of pioneer neuron growth cones in situ. *The Journal of cell biology* 1991;115:381–395. [PubMed: 1918146]
- Schaefer AW, Kabir N, Forscher P. Filopodia and actin arcs guide the assembly and transport of two populations of microtubules with unique dynamic parameters in neuronal growth cones. *The Journal of cell biology* 2002;158:139–152. [PubMed: 12105186]
- Schmandke A, Schmandke A, Strittmatter SM. ROCK and Rho: biochemistry and neuronal functions of Rho-associated protein kinases. *Neuroscientist* 2007;13:454–469. [PubMed: 17901255]
- Suter DM, Errante LD, Belotserkovsky V, Forscher P. The Ig superfamily cell adhesion molecule, apCAM, mediates growth cone steering by substrate-cytoskeletal coupling. *The Journal of cell biology* 1998;141:227–240. [PubMed: 9531561]
- Suter DM, Forscher P. Substrate-cytoskeletal coupling as a mechanism for the regulation of growth cone motility and guidance. *J Neurobiol* 2000;44:97–113. [PubMed: 10934315]
- Suter DM, Forscher P. Transmission of growth cone traction force through apCAM-cytoskeletal linkages is regulated by Src family tyrosine kinase activity. *The Journal of cell biology* 2001;155:427–438. [PubMed: 11673478]
- Suter DM, Schaefer AW, Forscher P. Microtubule dynamics are necessary for SRC family kinase-dependent growth cone steering. *Curr Biol* 2004;14:1194–1199. [PubMed: 15242617]
- Tanaka E, Ho T, Kirschner MW. The role of microtubule dynamics in growth cone motility and axonal growth. *The Journal of cell biology* 1995;128:139–155. [PubMed: 7822411]
- Tanaka E, Kirschner MW. The role of microtubules in growth cone turning at substrate boundaries. *The Journal of cell biology* 1995;128:127–137. [PubMed: 7822410]
- Turney SG, Bridgman PC. Laminin stimulates and guides axonal outgrowth via growth cone myosin II activity. *Nature neuroscience* 2005;8:717–719.

- Vallotton P, Gupton SL, Waterman-Storer CM, Danuser G. Simultaneous mapping of filamentous actin flow and turnover in migrating cells by quantitative fluorescent speckle microscopy. *Proc Natl Acad Sci U S A* 2004;101:9660–9665. [PubMed: 15210979]
- Waterman-Storer CM, Desai A, Bulinski JC, Salmon ED. Fluorescent speckle microscopy, a method to visualize the dynamics of protein assemblies in living cells. *Curr Biol* 1998;8:1227–1230. [PubMed: 9811609]
- Williamson T, Gordon-Weeks PR, Schachner M, Taylor J. Microtubule reorganization is obligatory for growth cone turning. *Proc Natl Acad Sci U S A* 1996;93:15221–15226. [PubMed: 8986791]
- Wylie SR, Wu PJ, Patel H, Chantler PD. A conventional myosin motor drives neurite outgrowth. *Proc Natl Acad Sci U S A* 1998;95:12967–12972. [PubMed: 9789024]
- Zhang XF, Schaefer AW, Burnette DT, Schoonderwoert VT, Forscher P. Rho-dependent contractile responses in the neuronal growth cone are independent of classical peripheral retrograde actin flow. *Neuron* 2003;40:931–944. [PubMed: 14659092]
- Zhou FQ, Waterman-Storer CM, Cohan CS. Focal loss of actin bundles causes microtubule redistribution and growth cone turning. *The Journal of cell biology* 2002;157:839–849. [PubMed: 12034775]

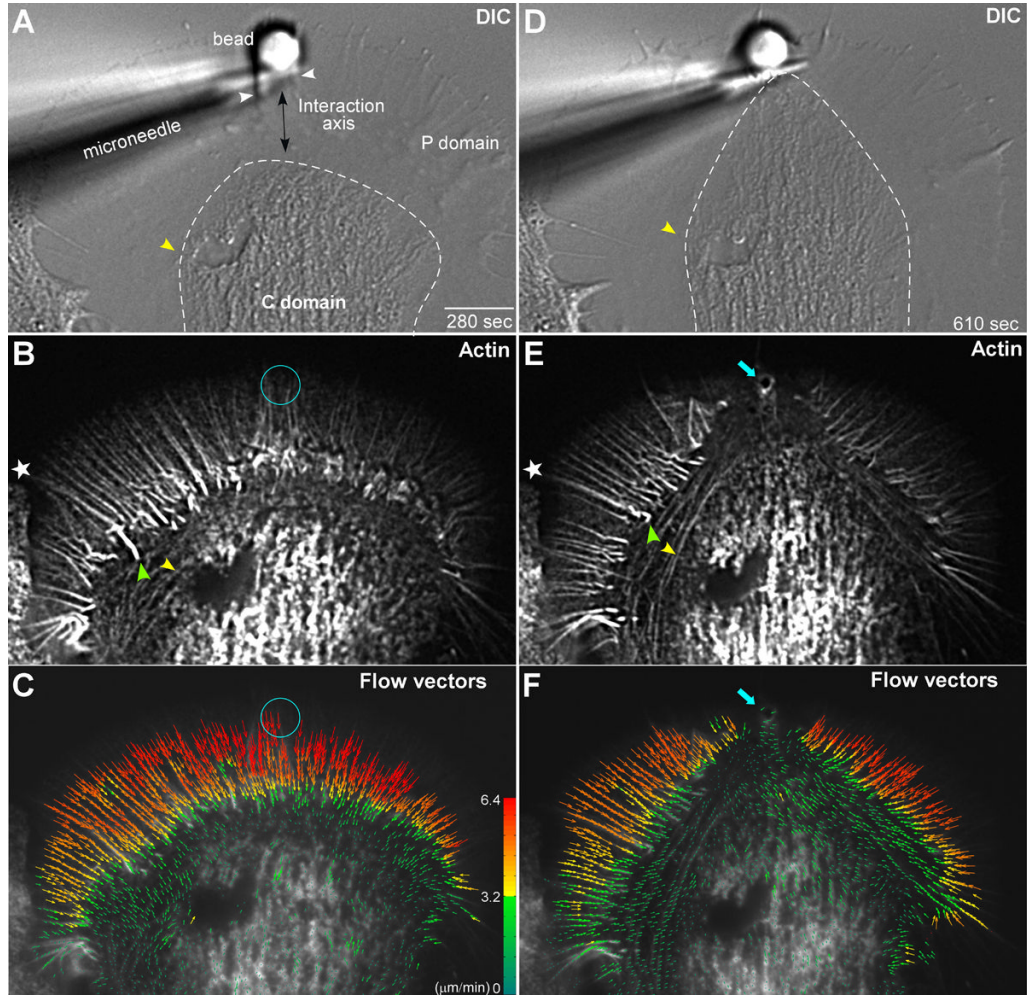


Figure 1. Actin Filament Network Remodeling Underlies Substrate Targeted Growth
 Left column shows (A) DIC, as well as corresponding (B) actin filament FSM and (C) actin filament flow vector map images of a growth cone for a time-point 280 seconds after placement and restraint of an apCAM coated target bead. White arrowheads in (A) demarks intrapodia. Double headed arrow in (A) indicates target interaction axis. Right column shows (D) DIC, (E) actin filament FSM, and (F) flow vector map images of the same growth cone 610 seconds after bead restraint following the C-domain growth response. Dashed white lines in (A and D) outline the C-domain organelle boundary. Star marks filopodial actin rib in P-domain and green arrow head filopodial root in T-zone (B and E). Yellow arrowheads in (A, B, D, and E) denote the position of actin arcs surrounding the C-domain organelles. Turquoise circles in (B) and (C) mark bead site and turquoise arrows in (E) and (F) show actin filaments accumulated at the new adhesion site. In (C) and (F) Colors encode flow speed in $\mu\text{m min}^{-1}$; and vector arrows, flow direction. Scale bar, 10 μm .

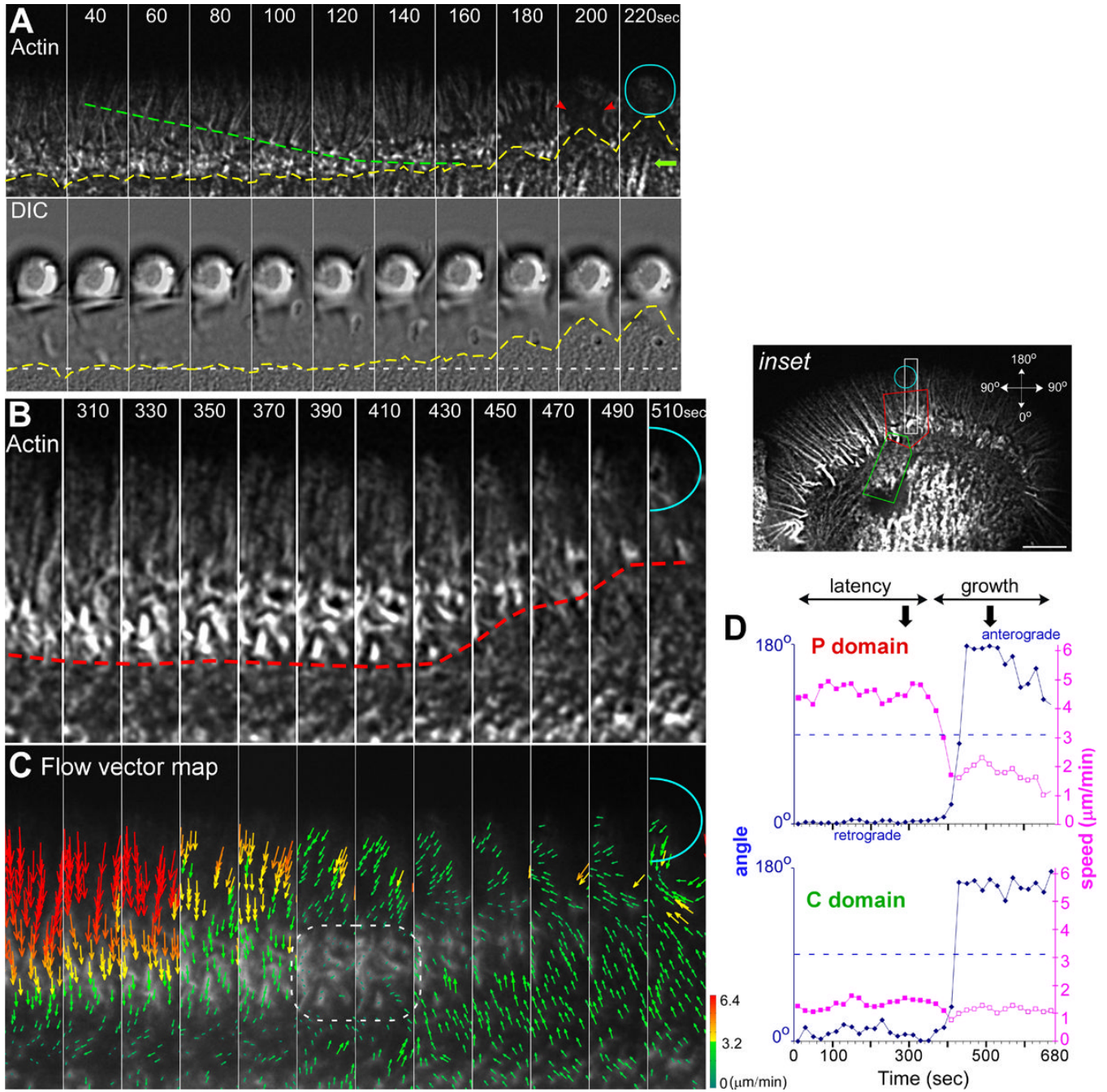


Figure 2. Retrograde Actin Flow Slows Concomitantly with Remodeling of Actin from the C-domain Engagement Corridor

Actin filament clearance in the P-domain precedes C-domain organelle engagement. (A) Actin filament FSM dynamics (top panel) and corresponding DIC (bottom panel) time-lapse sequence of a targeted growth response. Dashed green line denotes actin filament flow and yellow dashed lines mark the extending C-domain organelle boundary. Red arrow heads denote clearance of actin bundles from growth corridor. Green arrow denotes C-domain associated actin structures. (B) Actin filament FSM time-lapse sequence and corresponding (C) flow vector maps of a targeted growth response from white rectangle region of interest shown in the inset of Figure 1B. Red hatched line marks filopodial turnover in the T-zone. White dashed

region (C) shows an area with actin structure and strong flow attenuation during the growth phase. (D) Graphs plot the average speed and direction of flow over time in the target interaction corridor in the P-domain (red box, inset) and C-domain (green box, inset), respectively. Blue line and diamonds indicate the net direction of movement where 0° represents retrograde flow and 180° , flow towards bead site. Purple line and filled squares denote flow speed in the retrograde direction, whereas open purple squares designate anterograde flow speed towards adhesion site. Arrowheads in (D) denote the time interval shown in (B and C). Turquoise circles in (A, B, and C) mark bead site. Scale bar, $10\ \mu\text{m}$. The regions of interest in (A) and (B) are 27×5.4 and $22 \times 3\ \mu\text{m}$ respectively.

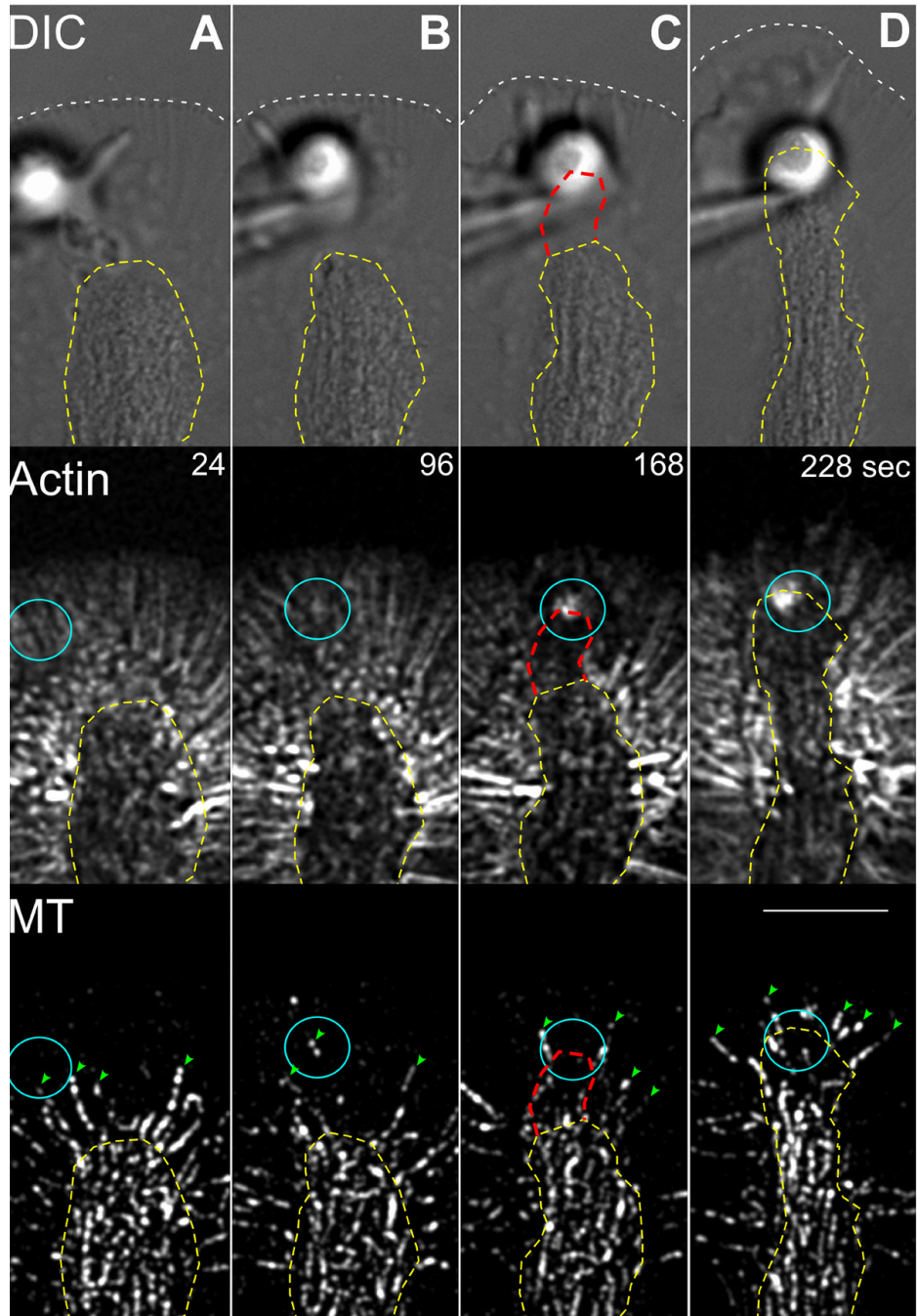


Figure 3. Actin Remodeling Precedes MT Advance

Columns (A-D) show a multimode time-lapse sequence of a targeted growth response; DIC (top panel), actin filament FSM (middle panel), and MT FSM (bottom panel). White hatched lines denote boundary of leading edge. Yellow hatched lines mark C-domain organelle border. Columns (A) and (B) show the latency period. Note the presence of filopodial actin bundles before growth corridor formation and dynamic P-domain MTs (green arrow heads). Columns (C) and (D) show the engorgement response. Note the reduction in actin bundles in the corridor (denoted by hatched red line in C) followed by C-domain MT invasion and advance of the leading edge. Turquoise circles mark bead site. Scale bar, 10 μ m.

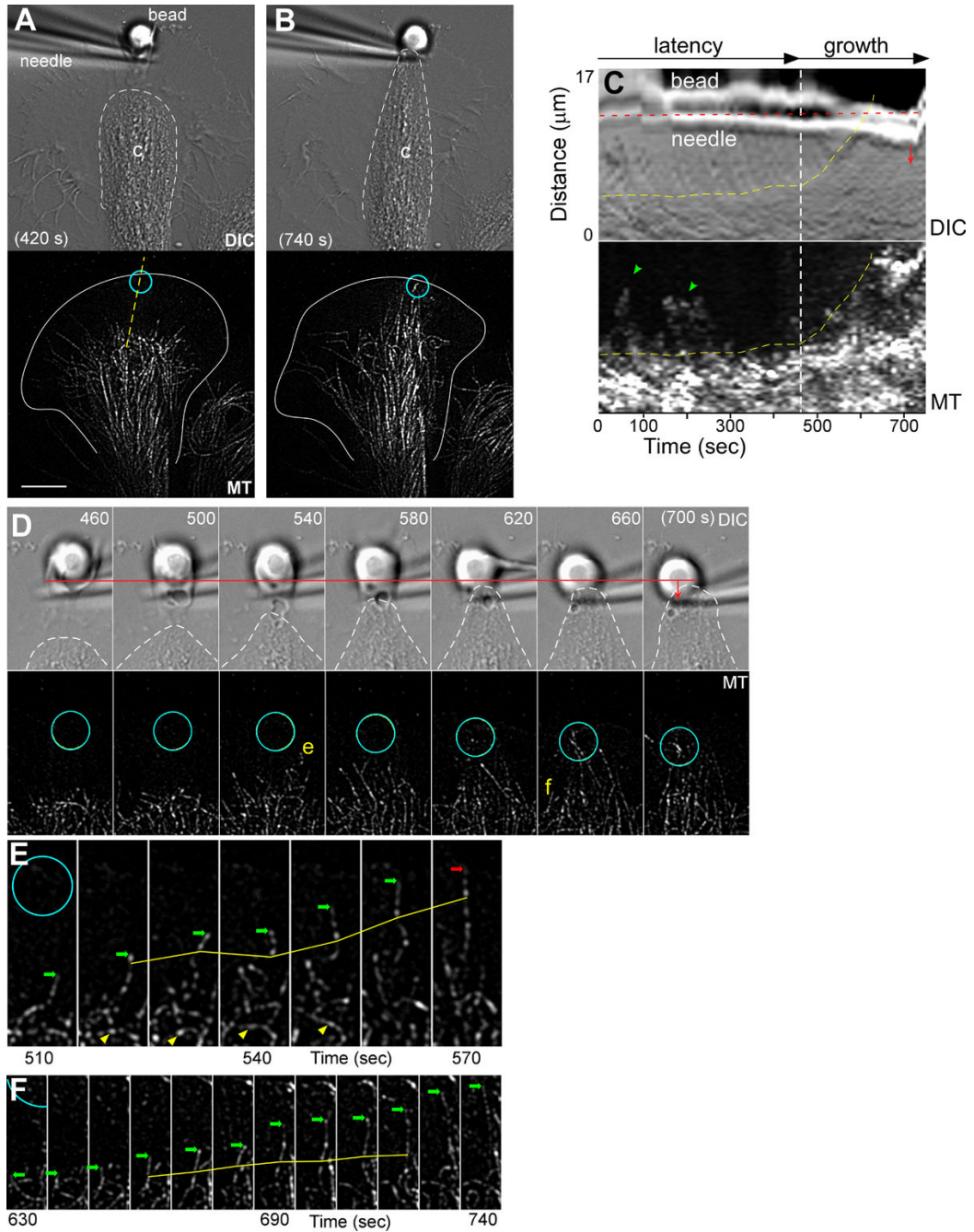


Figure 4. C-domain MTs Advance by Translocation and Polymerization during Substrate Evoked Growth

(A) DIC (top panel) and corresponding MT FSM (bottom panel) time-lapse images of a growth cone 420 seconds after placement and restraint of an apCAM coated target bead. (B) DIC (top panel) and MT FSM (bottom panel) images of the same growth cone later in time during the growth phase. Dashed white lines outline the C-domain organelle boundary and turquoise circles denote the bead site. (C) Kymograph analysis of the region of interest marked by yellow line in (A); DIC channel (top panel) and MT channel (bottom panel). In (C): yellow dashed lines mark the organelle boundary; green arrow heads highlight dynamic MTs interrogating the target interaction site during the latency period; and red dashed line denotes the initial

needle position. The needle is pulled away from the growth cone at the 720 second time point. (D) DIC (top) and MT (bottom) time-lapse montages of the target interaction corridor. White dashed line marks organelle boundary. The initial position of the bead is marked by red line with arrow showing displacement of bead and needle towards the C-domain during the targeting response. (E) and (F) show time-lapse montages of single MTs from the interaction corridor. Green arrows identify the terminal speckles of the growing MTs while the solid yellow lines mark internal reference speckles. Red arrow in (F) identifies a MT shortening event. Yellow arrow head in (E) marks un-looping MT. Scale bar, 10 μm .

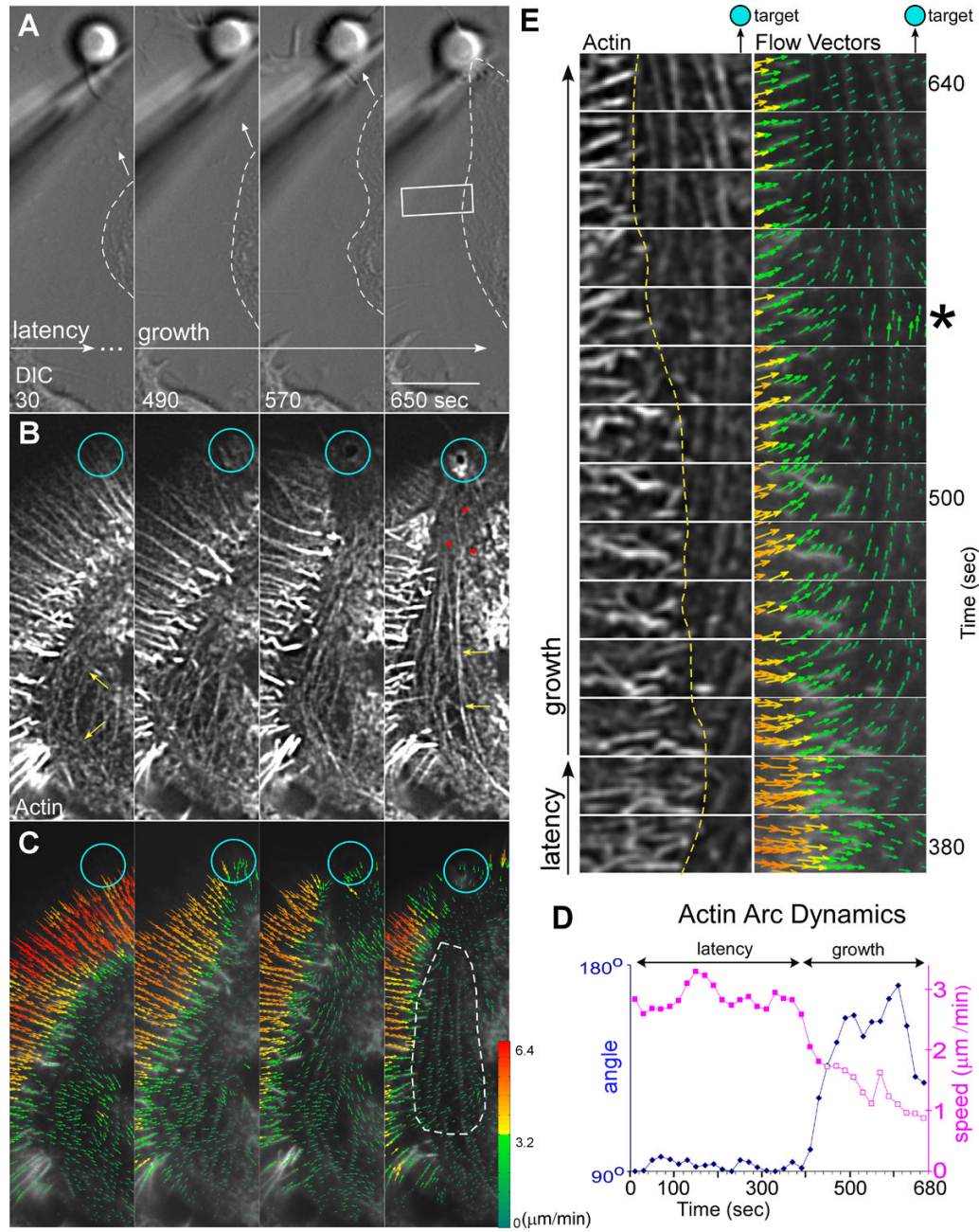
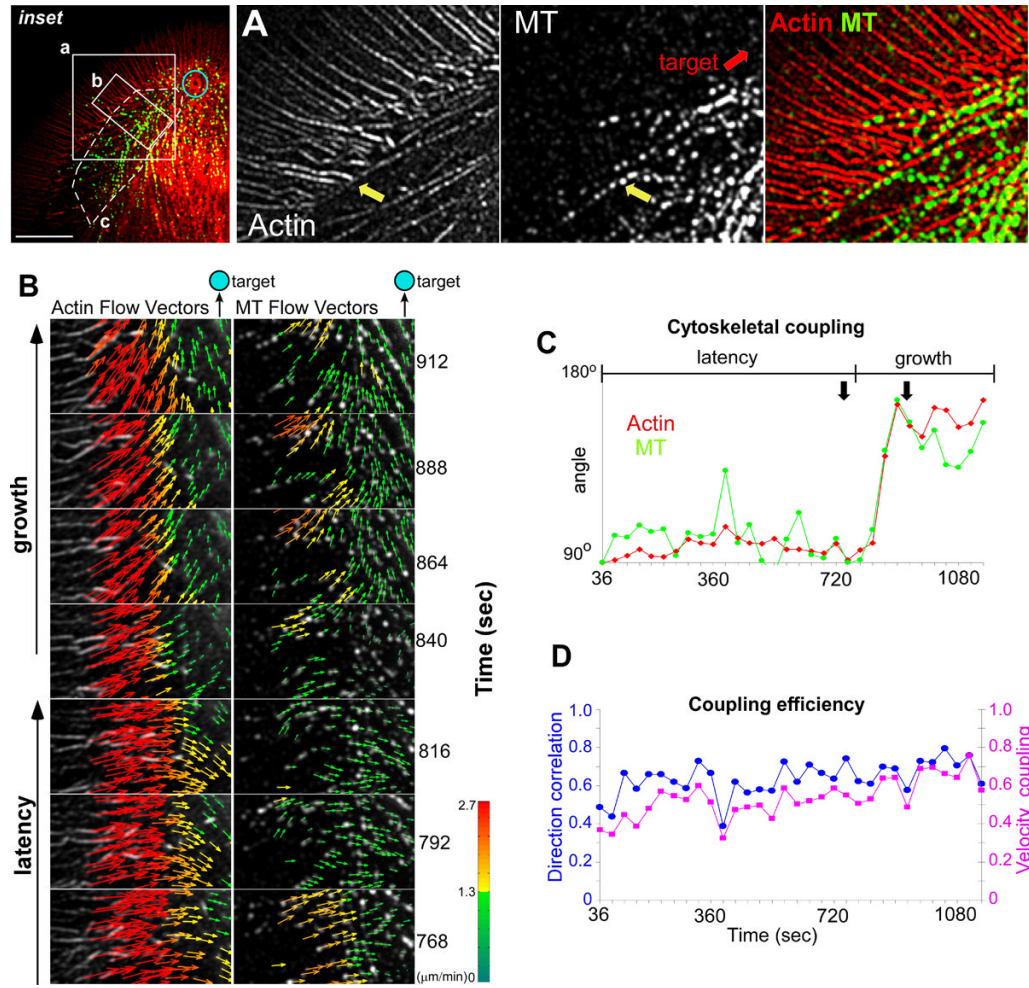


Figure 5. Actin Arcs Couple to the Adhesion Site Shaping the C-domain Engorgement Response (A) DIC and corresponding (B) actin filament FSM and (C) flow vector map time-lapse montage taken from the left side lateral aspects of the growth cone in Figure 1. Dashed lines outline C-domain in (A). Yellow arrows in first and last frame of (B) show straightening of normally curved arcs and red arrow heads show arcs embedded in actin meshwork in the target interaction corridor. Turquoise circles in (A, B, and C) show bead site. (D) Graph of the average flow speed and direction for the arcs in the white hatched region of interest in (C). Blue line and diamonds indicate direction where 90° represents retrograde flow and 180° , flow towards bead site. Purple lines and filled squares denote arc speed towards the C-domain whereas open purple squares designate speed towards adhesion site. (E) Time-lapse sequence of region outlined by white box in (A) showing the actin channel (left) and flow vector map (right).

Yellow hatched line marks T-zone boundary and star denotes time-point showing arc vector angles perpendicular to peripheral flow. Scale bar, 10 μm .



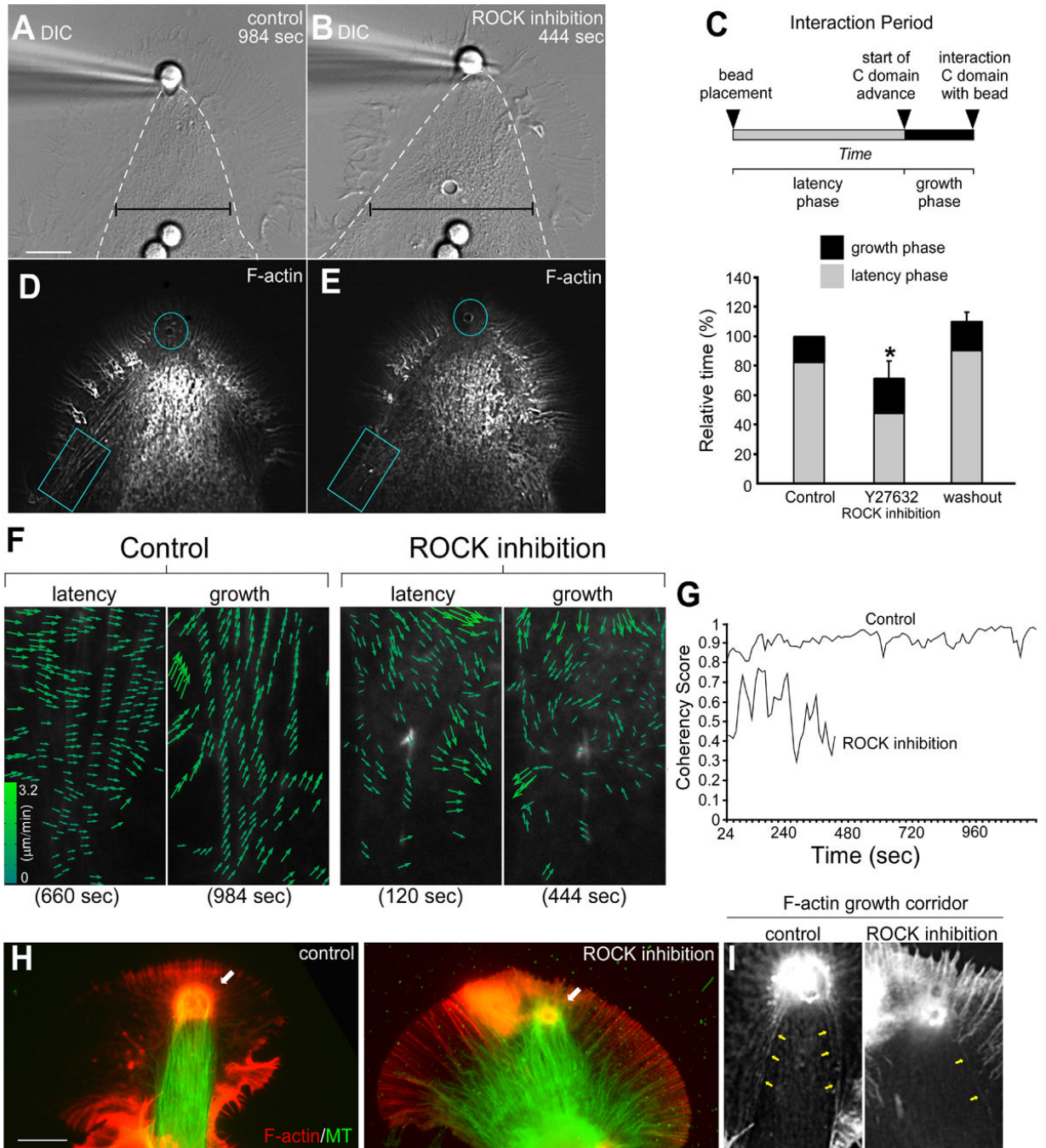


Figure 7. Arc Disruption Promotes C-domain Engorgement while Inhibiting Consolidation
 (A) DIC image of a control substrate evoked growth response 984 sec after apCAM bead placement and restraint. (B) DIC image of the targeting response of the same growth cone following a 20 minute pretreatment with 20 μ m of the Rho Kinase inhibitor Y27632, 444 sec after bead placement. Hatched white lines in (A and B) mark the C-domain organelle boundary. Note the spread appearance of the C-domain during the targeting response following drug treatment (black calipers). (C) Schematic of growth response stages (top). Graph (bottom) shows Rho Kinase inhibition reversibly decreased ($69.4\% \pm 6.0\%$ of controls) the latency phase. Data are expressed as mean \pm SEM. Statistical analysis was performed with two-tailed paired t-test. * indicates $p < 0.01$; $n=7$. (D and E) Actin filament FSM images of the

corresponding control and drug treatment at time points shown in (A) and (B). (F) Flow vector maps from turquoise box regions of interest in (D, control) and (E, treatment) showing latency and growth time points. (G) Graph shows the reduced coherency of the F-actin vectors in drug treatment versus control over time. A coherency score of one means all vectors are parallel and close to 0 if their directions are random. (H) F-actin/MT immunofluorescence images showing control (left panel) and Rho Kinase inhibited (right panel) targeted growth responses. (I) F-actin immunofluorescence Images showing the growth corridors from (H). Yellow arrows mark arcs surrounding the growth corridor. Turquoise circles mark bead site in (D and E). Scale bar is 10 μm .

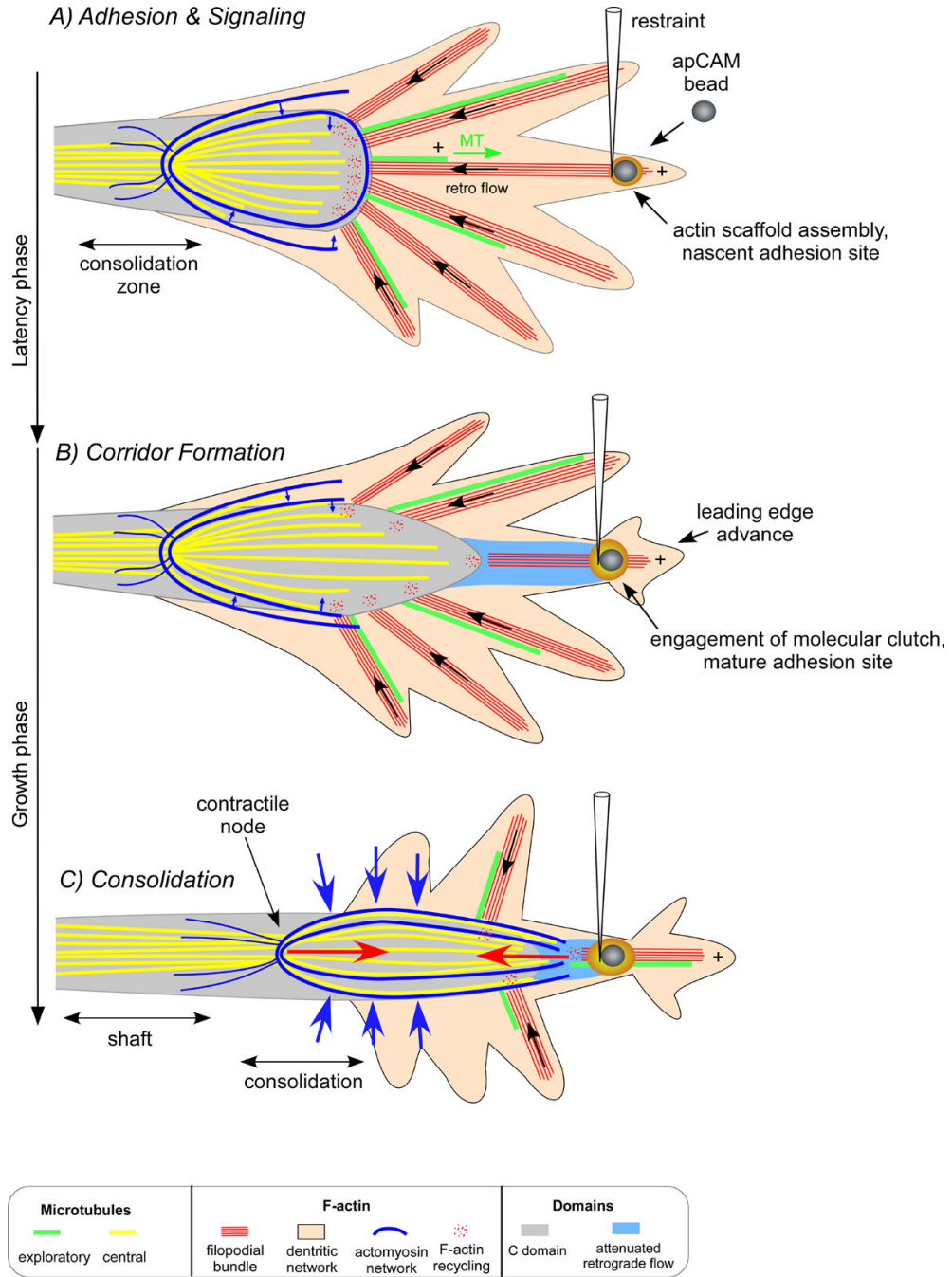


Figure 8. Neurite Growth Model

Cytoskeletal response underlying substrate evoked growth. A) The “latency” phase begins after bead restraint and is characterized by localized actin assembly near the bead binding site which acts as a scaffold for docking signaling proteins. During this time, filopodial actin bundles (red) and the less polarized actin network (pink) move by fast retrograde flow in the P domain (black arrow). Dynamic MTs (green) enter the P domain by polymerizing parallel to filopodia. MTs are simultaneously carried rearward by tight coupling to retrograde flow and do not accumulate at the nascent adhesion site. MTs in the C-domain (yellow) are restricted by interactions with actomyosin arcs (blue). B) The start of the “growth phase” is marked by strengthening of the adhesion site and engagement of the molecular clutch. Flow slows in the interaction corridor

(blue zone) and is accompanied by actin filament restructuring and continued actin recycling. This process removes a barrier to C-domain (outlined gray zone) advance towards the adhesion site. C) Later, tension develops (red arrows) between the restrained bead substrate and contractile arcs, causing arcs to straighten and compress MTs into the C-domain (blue arrows). We hypothesize this action facilitates MT bundling and subsequent cross-linking necessary for consolidation of a new segment of the axon shaft.